Extraction of signals from linear topological defects

Jeffrey Morais, Mattéo Blamart, Robert Brandenberger

Abstract

We consider the logistics behind observing the signal of a linear U(1) topological defect (cosmic string) in a noisy background given by the ΛCDM cosmological perturbations. We investigate quantum field theories admitting these topological defects and describe their stability via homotopy groups. We characterize the different conditions on the formation and evolution of cosmic strings using the Kibble mechanism and the scaling solution with an emphasis of working in redshift space for the string wake. We focus on statistics to enhance and isolate the signal of the string from ambient noise. It is found in the regime $G\mu \sim 3 \times 10^{-7}$ that a 1D match filter after unfolding the temperature matrix into an array shows a clear indication for what a string signal observation looks like. We also demonstrate the domain in which the string signal is bounded by.

1 Introduction

A topological defect is defined as a solution to a quantum field theory which is homotopically distinct from the vacuum solution, usually coming from discontinuities in boundary conditions of a set of fibrations [1]. We consider as an example a gauge theory with non-commuting group elements, which is given by the Yang-Mills action coupled to spinors and scalar fields that describes the interactions between fermions, gauge bosons, and bosons [2]:

$$S = -\frac{1}{2}\int_M \mathrm{tr}(F \wedge \star F) + \int d^4y \left[\bar{\psi}(i\not{D} - m)\psi + \frac{1}{2} D_\mu \phi D^\mu \phi - V[A,\phi] \right] \tag{1}$$

Here the first term is the gauge invariant second Chern form $(F^a_{\mu\nu})^2$ [3] integrated over a manifold M, where $F^a_{\mu\nu} = \partial_\mu A^a_\nu - \partial_\nu A^a_\mu + g f^a_{bc} A^b_\mu A^c_\nu$ is the curvature 2-form for a non-Abelian gauge theory, f^{abc} are the structure constants of the underlying symmetry group G, $D_\mu = \partial_\mu - igA^a_\mu t_a$ is the covariant derivative with an associated connection A^a_μ defined on a G-bundle, t_a are the generators of G (sometimes instead replaced by the irreducible representations of the group denoted as t^a_r), ψ is an N-component fermion spinor, m is the mass of the fermion, ϕ is a scalar field, and $V[A,\phi]$ is a functional potential including interacting terms with an implicit coupling constant g, as well as non-interacting terms. This theory has associated local gauge and phase symmetries in the fermion spinors and scalar fields, respectively given by:

$$\psi \longrightarrow \exp\left(i\alpha^a t_a\right)\psi, \quad \phi \longrightarrow e^{i\beta}\phi \tag{2}$$

where α^a are coefficients contracted with the generators, and $\beta \in \mathbb{Z}$. At certain energy scales or below certain temperatures, the scalar symmetry may be broken spontaneously during a phase transition. The

field which is defined as the symmetry breaking parameter (in our case the scalar field ϕ) has an associated potential only depending on itself $V(\phi) \subset V[A, \phi]$ which changes during the phase transition, usually occurring in the decay of a false vacuum via bubble nucleation. The minimum of the potential is denoted as the vacuum manifold $M \coloneqq \min_{\phi} V(\phi)$ and discontinuities in fields defined on it is what leads to the formation of topological defects and will be useful in describing homotopy groups for stability conditions of the defects.

2 Stability conditions of topological defects

2.1 Homotopy classes

Depending on the system, one can have multiple phase transitions and thus the formation of multiple singular or composite topological defects. This is characterized by a symmetry breaking pattern in which the underlying symmetry group G reduces to a subgroup of itself H (usually the isotropy subgroup) and so forth, denoted by the following:

$$G \longrightarrow H \longrightarrow \dots \tag{3}$$

As an example, one can consider a grand unified theory with a unified gauge group $SU(5)$ which is spontaneously broken into a unitary product group seen as:

$$SU(5) \longrightarrow SU(3) \times SU(2) \times U(1). \tag{4}$$

During each step in the symmetry breaking pattern we can look at the stability condition of the defect to see whether or not the theory admits them. To do so, it is useful to define a homeomorphism between M and the quotient space G/H given by $M \simeq G/H$ in which the elements $g \in G$ are mapped to the left cosets of H in G, given by $\{gh\}$ where $h \in H$ [3]. Next, we must consider homotopy groups which characterize topological spaces. Consider an equivalence class of maps that map from an n-sphere S^n to another space X, under the condition that a base point is preserved in the mapping. The equivalence class of these maps are known as homotopy classes. Two maps within this class γ_1, γ_2 are homotopically equivalent if they can be continuously deformed into one another via a continuous one parameter family of maps to adhere to the condition [4]:

$$\gamma(t) : S^n \to X \mid t \in [0, 1],\ \gamma(0) = \gamma_1,\ \gamma(1) = \gamma_2 \tag{5}$$

The homotopy classes form a group called the n'th homotopy group[†] of a topological space X, denoted $\pi_n(X)$, defined as the set of all homotopy classes of maps $f_k : S^n \to X$ [5].

This is somewhat physically unintuitive, so for clarity we will consider some specific examples. The first homotopy group $\pi_1(X)$ is known as the fundamental group of a topological space, and is the group of equivalence classes under homotopy of loops within X. The non-triviality of this group gives rise to cosmic string defects. Moreover, the second homotopy group $\pi_2(X)$ is the group of homotopy classes of closed two

[†]As a side note, $\pi_n(X)$ is a group for $n \geq 1$ and $\pi_0(X)$ is only a set.

dimensional surfaces in X [6]. The triviality of this group gives rises to monopole defects. This intuition can be extended for all n.

2.2 Exact sequences

For the case of topological defects, we shift our focus to homotopy groups defined on the vacuum manifold M denoted $\pi_n(M)$. In general, a theory admits a local or global topologically stable defect if the homotopy group is non-trivial, meaning it obeys the condition [7]:

$$\pi_n(M) \neq \mathbb{1},\ n \in \mathbb{Z}. \tag{6}$$

Stability conditions however are often more specific than the statement above, dealing with the nature of the vacuum manifold, and the symmetry group manifold.[‡] The computations of these conditions and the homotopy groups are derived efficiently from exact sequences.

For maps $f : A \to B$, $k : B \to C$ mapping between topological spaces A, B, C, the sequence $A \to B \to C$ is *exact* if and only if the image of f coincides with the kernel of k. This is visualized in the following figure:

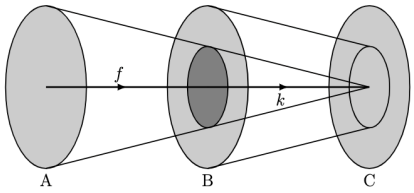

Figure 1: Visualization of an exact sequence of functions mapping between various topological spaces. The shaded region within the space B represents the kernel of k and the image of f. [7]

We can consider a longer sequence of maps that are exact at every intermediate point. In our case we will consider an injection map from the subgroup H to the symmetry group G and a projective map from G to $G/H \simeq M$, defined respectively as:

$$\begin{aligned} i_* : \pi_n(M) &\to \pi_n(G) \\ p_* : \pi_n(G) &\to \pi_n(G/H). \end{aligned} \tag{7}$$

This gives us a set of n-corresponding maps for our large exact sequence between homotopy groups of the same n. Furthermore, we may also have sequences that map between homotopy groups of different n. Consider a fibre bundle where the base space is G and the projected space is G/H. We can lift a loop living in G/H to a loop in G, and since the loop returns to a starting point, the curve must end at an element of H. This is visualized in the following image:

[‡]It is noted that in this paper, all symmetry groups are taken to be Lie groups, thus they are also manifolds.

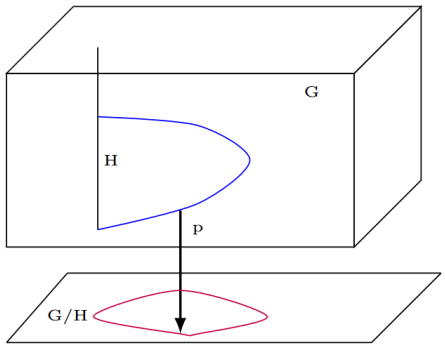

Figure 2: Lifting a curve (red) from the projected space to a curve (blue) in the base space in a fibre bundle via the inverse of the projective map p. [7]

If the final element of the curve in H belongs to the same component as the identity, we can deform it continuously until the endpoints is the identity, and the curve forms a loop in G. Each homotopy class of loops in G/H defines a component of H, so we can generally have another map from G/H to H:

$$\partial : \pi_n(G/H) \to \pi_{n-1}(H) \tag{8}$$

From the sets of maps we have above, we can construct a long exact sequence of mapes terminating at $\pi_0(G/H)$:

$$\begin{aligned} \cdots \longrightarrow \pi_2(G) \longrightarrow \pi_2(G/H) \longrightarrow \pi_1(H) \longrightarrow \pi_1(G) \longrightarrow \\ \pi_1(G/H) \longrightarrow \pi_0(H) \longrightarrow \pi_0(G) \longrightarrow \pi_0(G/H) \end{aligned} \tag{9}$$

How does this exact sequence help us recover stability conditions of topological defects? Using the condition that the phase transitions form an exact sequence, we can impose certain conditions to reduce the sequence that will give us relations between homotopy groups [7]. Consider the following final conditions.

It occurs that for a Lie group G, the second homotopy group is trivial, i.e. $\pi_2(G) = \mathbb{1}$. Moreover, if the fundamental group of G is non-trivial, meaning G is simply connected, we can replace G by its universal covering group $\tilde{G}$. Finally, from the conditions previously mentioned, if we have a sequence structure that looks like $1 \to A \to B \to 1$ and $A \simeq B$, the sequence reduces to the stability condition of a monopole [7]:

$$\pi_2(G/H) = \pi_1(\tilde{H}) \tag{10}$$

The above states that the theory admits topologically stable monopoles if the universal covering of the subgroup H is non-simply connected. Furthermore, if we restrict G to the connected part of itself G_0 and define the connected part of the subgroup $H_0 = H \cap G_0$, then we have a condition on cosmic strings:

$$\pi_1(G/H) = \pi_0(\tilde{H}_0) \tag{11}$$

The above states that topologically stable cosmic strings exist if $\tilde{H}_0$ has disconnected pieces. Now we have described the stability conditions for topological defects, in particular cosmic strings, we move on to

describing the formation of cosmic strings from a specific scalar field symmetry breaking potential $V(\phi)$. It is noted that for the stability conditions of composite defects, *relative* homotopy groups are used such as $\pi_n(M, M')$, but this won't be covered in this paper.

3 Linear defects: cosmic strings

Now for the purposes of this paper we shift our focus to the linear topological defect relating to the fundamental group $\pi_1(M)$ of the vacuum manifold, cosmic strings. These are defects formed in a phase early universe between recombination and reheating, and their signal persists to our current time. Cosmic strings are of particular interest as their mass energy density μ is quadratically proportional to the energy symmetry breaking scale η and thus allows us to probe particle physics models at very high energy scales relevant to structure formation [8].

To model cosmic strings, we consider an Abelian theory where we take the G-bundle to be a principal U(1) bundle, and we have the reductions: $A^a_\mu \to A_\mu$, $F^a_{\mu\nu} \to F_{\mu\nu} = \partial_\mu A_\nu - \partial_\nu A_\mu$, & $D_\mu \to \partial_\mu + ieA_\mu$. Moreover, to model cosmic strings we will consider the interaction between spin-0 bosons and gauge fields, modelled with scalar fields ϕ and vector fields A_μ, respectively. With this we can write an action of this theory with a U(1) phase symmetry $\phi \to e^{i\alpha}\phi$:

$$S = \int d^4y \, \frac{1}{2} D_\mu \phi D^\mu \phi + \frac{1}{4} F_{\mu\nu} F^{\mu\nu} - V(\phi). \tag{12}$$

Here the potential is a symmetry breaking potential with the form: $V(\phi) = \frac{1}{4}\lambda(\phi^*\phi - \eta^2)^2$, where λ is the interaction coupling constant and η is the symmetry breaking scale. What is special about this potential is that above a critical temperature $T_c \sim \eta$ we have a symmetric state that rests within a global minima but below this critical temperature this minima becomes a local maxima meaning a false vacuum, and we move towards a metastable antisymmetric state [9]. During this temperature transition spontaneous symmetry breaking occurs whereby the system has a symmetry not shared by its ground state, implying a degeneracy in the vacuum state $\langle\phi\rangle$. The resulting potential is known as the Goldstone potential and has the following shape:

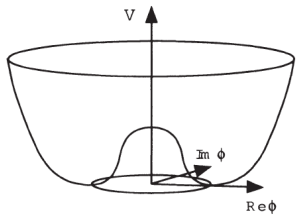

Figure 3: Symmetry breaking Goldstone potential defined over the complex scalar field plane. The minima of the potential, the vacuum manifold, is a circle $M \simeq S^1$. [7]

During the phase transition, it can be derived from finite temperature field theory that the potential obtains a finite temperature correction of the form:

$$\Delta T = \frac{1}{2}\bar{\lambda}T^2|\phi|^2, \tag{13}$$

where $\bar{\lambda}$ is the interaction coupling constant rescaled to absorb boundary conditions on the variance of the scalar field, and T is the system temperature. The analogue to this correction in a quantum field theory would be finite loop-order corrections from the interactions of spin-0 bosons.

Moreover, the degenerate vacua along the circle are labelled by a phase angle α given by [9]:

$$\langle\phi\rangle = e^{i\alpha}\eta/\sqrt{2} \tag{14}$$

During the decay of the false vacuum, through bubble nucleation two bubbles form (these bubbles are domain walls, which are topological defects for $\pi_0(M)$) with a positive surface tension, and their intersection by continuity requires the scalar field to vanish within the closure of the vacuum manifold circle [10]. At center of the circle, known as the core, the field has to go through a central hump in the potential and has a potential energy of $\mathcal{O}(T_c^4)$. Everywhere else outside this core point, the energy quickly dissipates as the universe expands so we say the energy is trapped within the point [7]. Moreover, in theories such as the Abelian-Higgs model, we can have string configurations which are translationally invariant, and thus this trapped energy occurs for points above and below the core. Connecting these points gives use a line of trapped potential energy which is the cosmic string. Cosmic strings don't have ends and don't break, thus either occur as infinite length strings in nature (bounded by the event horizon of our expanding universe), or loops.

Cosmic strings possibly have significant effects on large-scale density distributions and anisotropies in the CMB. Furthermore, we can contract the energy mass density with Newton's gravitational constant to get a dimensionless quantity $G\mu$ known as the string tension, which will be crucial in cosmological observations and computing upper limits at high energy scales. In the next section, before moving on to modelling cosmic strings in redshift space, we look at some conditions on the distribution and size of the string based on the Kibble mechanism.

4 Cosmic string evolution and properties

4.1 Correlation lengths

An important condition on the distribution of cosmic strings comes from correlation lengths. A useful model in computing the correlation length between cosmic string phases is the Kibble mechanism [4]. In this model we have a lattice of points where at each site a rod confined to a plane is pivoted off the vertical axis by an angle of ϕ, free to oscillate and rotate, and the tip of the rods are connected to other rod tips via springs. The spring is analogous to the covariant derivative terms in the cosmic string action. Furthermore, the potential for the system $V(\phi)$ is modelled via Newtonian gravity with $\phi \in [0, \pi/2]$, thus this model is analogous to the scalar field model with the potential $V(\phi) = \frac{1}{4}\lambda(|\phi|^2 - \eta^2)^2$.

For $T >> T_c$, where T_c is the critical temperature of the system, all rods undergo large amplitude and high frequency oscillations. The phases of oscillations with large separations are uncorrelated and the length

beyond which the phases are uncorrelated is the correlation length ξ. It follows by causality that there is an upper bound on the correlation length given by [4]:

$$\xi(t_c) < t_c. \tag{15}$$

Here t_c is the causal horizon length at T_c (recall we are using natural units). Now for cosmic strings, the boundaries between correlated phases become topological defects (domain walls) and thus during a phase transition we will have a networks of defects with mean separation of $\xi(t) \leq t$. Moreover, this tells us that there are no correlations on scales larger than t can be established. Correlation lengths can moreover be interpreted as the mean curvature radius of string loops and separation lengths of long strings.

4.2 Scaling solution & loop formation

Recall from the last section that the Kibble mechanism tells use after a phase transition in the early universe, a network of cosmic strings will persist with a separation length of $\xi(t)$. String loops with radii equal to the correlation separation length can form via the intersection of two infinite length cosmic strings (by exchanging ends), and when formed the loops shrink via oscillation due to the string tension and they decay via gravitational radiation [4]. Moreover, string loops can also be formed via self intersection. The process of loop formation is visualized in the following figure:

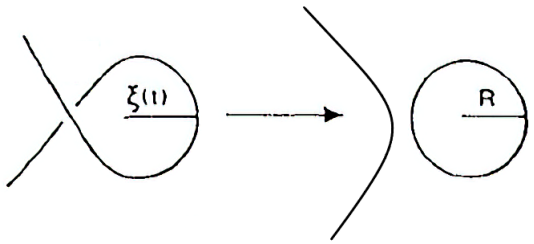

Figure 4: Formation of cosmic string loops via self intersection. [4]

Both processes outline a mechanism by which the infinite length cosmic string network loses energy. Moreover it can be shown that as a consequence, the correlation length of the string network is proportional to its causality limit:

$$\xi(t) \sim t. \tag{16}$$

From this it can be concluded that the fraction of the energy density of the infinite cosmic string network $\rho_\infty(t)$ to the background energy density $\rho_c(t)$ is fixed and in fact is proportional to the string tension [4]:

$$\frac{\rho_\infty(t)}{\rho_c(t)} \sim G\mu. \tag{17}$$

We see from above that the cosmic string network approaches a *scaling solution* in which the statistical properties of the network are independent of time if all distances are scaled to the horizon distance (Hubble length t). Alternatively, this can be interpreted as the distribution of cosmic strings is scale invariant due to

the rate at which cosmic strings form loops and lose energy. From this it suffices in our model to populate a single cosmic string per Hubble volume.

4.3 Cosmic string wakes & anisotropies in the CMB

As cosmic string relativistically move through space or plasma, much like boats in the sea, it creates a wake which gives rise to velocity perturbations. Due to the fact that the string has equal tension and a uniform length energy density, a gravitational lensing effect causes a conical structure to form in the space orthogonal to the string [11]. We can then unwrap this cone onto a plane and we are left with the deficit angle of which the wake spans. The velocity perturbations from the wake can be seen in the rest from of the cosmic string, whereby plasma moves towards the back of the wake, which can be seen in the following figure:

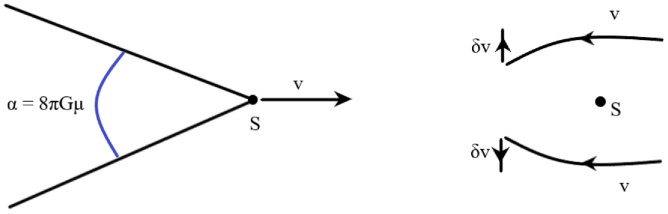

Figure 5: Wakes formed by the movement of cosmic strings moving through plasma. The left piece shows the string wake with the width of given by the deficit angle α. The right piece shows the same process in the rest frame of the cosmic string where the velocity perturbations δv can be seen going towards the back of the wake. [4]

The width of the wake is given by the deficit angle $\alpha = 8\pi G\mu$ where $G\mu$ is the dimensionless string tension. As the string moves through plasma or a bath of dark matter, it induces velocity perturbations given by:

$$\delta v = 4\pi G\mu v\gamma(v), \tag{18}$$

where v is the velocity of the wake and $\gamma(v)$ is the associated relativistic gamma factor. This induces *planar overdensities* for times past the time of equal matter and radiation t_{eq}.

What is the relevance of cosmic string wakes? These wakes give rise to anisotropies in the cosmic microwave background (CMB). As radiation passes through different sides of the wake there is a Doppler shift and thus a change in temperature. The change in temperature is a direct consequence of the deficit angle and would be negligible otherwise. This is visualized in the following:

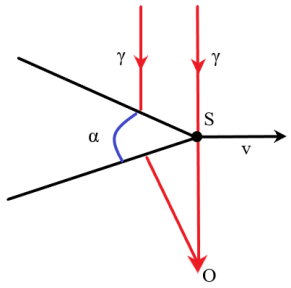

Figure 6: Anisotropy in CMB from the Doppler shift of radiation (red) passing on different sides of the cosmic string wake as a consequence of the deficit angle. [4]

The temperature variation caused by the process (normalized by the ambient temperature) is given by the equation:

$$\frac{\delta T}{T} \sim 8\pi G\mu v\gamma(v). \tag{19}$$

The following section will delve into modelling cosmic strings with finite lengths and an alternate mechanism of anisotropy in the CMB. Following that will be modelling the wake anisotropy signal in redshift space in Python.

5 Modelling cosmic strings in redshift space

5.1 Finite length model

For the purposes of our analysis, we will consider a single cosmic string wake being populated per Hubble volume. For this to work, we move from a network of infinite length cosmic strings to a set of straight cosmic string segments of finite length. These segments and their corresponding wakes have the following dimensions:

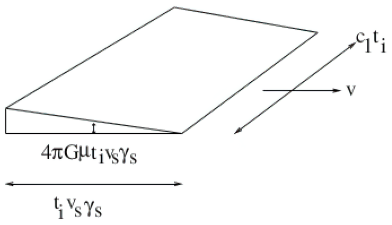

Figure 7: Dimensions of a cosmic string wake wedge, modelled with a finite length. [12]

Here c_1 is a real constant of order unity, t_i is the time of formation (taken to be at recombination), v_s is the velocity of the string and γ_s is the associated relativistic gamma factor. Next we consider the signal of the wake in 21 cm observations as a temperature variation or anisotropy in the CMB.

CMB radiation passes through the overdensities within the wake and is eventually emitted via the excitation of hydrogen within the wake [4] in quantized 21 cm packets. If the wake temperature emitted is colder than the ambient CMB photons from the surface of last scattering, then the wake absorbs CMB radiation at 21 cm and if hotter then it is emission. It is noted that a cosmic string will form near recombination, persist for a Hubble time, and dissipate but the wake persists to present time. As light is emitted from the front and back of the wake (along the lightcone connecting the present time to the time of formation of the cosmic string), there is a frequency shift $\delta\nu$ between the two emitted rays [8]. This can be translated into a brightness temperature variation δT_b, and is the characterization of the cosmic string signal, given by [13]:

$$\delta T_b(\nu) = [0.07K]\frac{x_c}{1+x_c}\left(1-\frac{T_\gamma}{T_{K/g}}\right)\frac{\sqrt{1+z}}{2\sin^2\theta}, \tag{20}$$

where x_c is the collision coefficient, T_γ is the temperature of the CMB photons prior to entering the gas cloud within the wake, $T_{K/g}$ is the kinetic temperature of the wake [†], z is the redshift, and θ is the angle off the line of sight from the observer to the wake. This gives us a wedge in physical space with a temperature gradient. Moreover from other analyses done [13], it is found that the wake signal is very narrow in the redshift direction. Thus the cosmic string signal is characterized by a wedge temperature gradient in physical space, that is narrow in redshift space. With this noted, we move on to constructing the wake temperature gradient in redshift space.

5.2 Construction of the wake

Now that we have described the signal of the wake, we can begin to build it in first in physical space. Consider a Hubble volume centered at the origin of a physical coordinate system. Within it we can construct a wake from six points, following the dimensions given in the previous section. It is noted the deficit angle is exaggerated to show the nature of the wake, which would otherwise look like a plane for actual values of the angle. A wedge in physical space within a Hubble volume will thus look like:

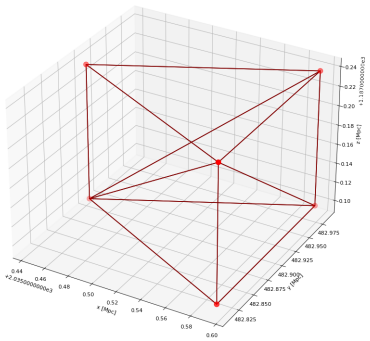

Figure 8: Wake wedge in physical coordinates.

[†]The subscript is in reference if shock heating or incoherent intrinsic gas thermal energy dominates which changes the amplitude.

Next, to make the wake configuration more arbitrary, we apply random rotations about all three axes. Following this, due to the redshift dependence of the brightness temperature, we would like for our vertical axis to be rescaled to a redshift axis. This rescaling relation between distance and redshift is implicitly found from the non-linear PDE solutions to Einstein's equations. The integral is non-elementary and is without an analytic solution even with the use of complex analysis or variational functional calculus, thus we proceed to generate the relationship numerically, which looks like:

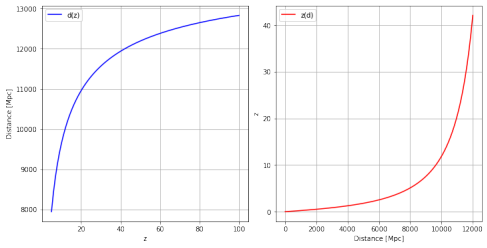

Figure 9: Relationship between redshift and distance scaling. The left plot shows distance as a function of redshift, while the right plot shows its inverse, redshift as a function of distance.

Using this we can rescale the vertical physical axis to a redshift axis. Finally we must take into account that in an expanding universe physical coordinates dilate. Thus to match cosmological observations, we convert from physical to comoving coordinates via the relation:

$$dx^{\mu}_{\text{phys}} = a(z)\, dx^{\mu}_{\text{com}}, \tag{21}$$

where $a(z)$ is the scaling factor for an expanding ambient spacetime. Using the scaling, dilation, and rotation transformations mentioned above, we have our wake in comoving-redshift space, which looks like:

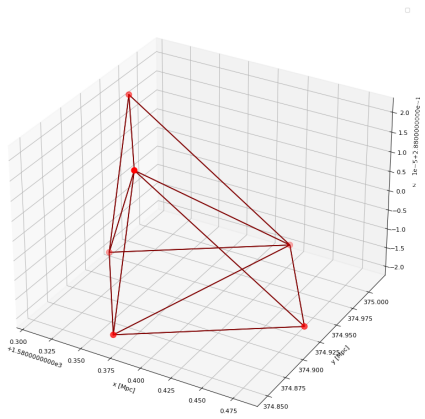

Figure 10: Wake wedge in comoving-redshift coordinates with an arbitrary orientation.

Next, using complex convex hull manifolds, we can cover the wedge in simplices and test whether points lie within the hull. Using a flooding technique, we fill the Hubble volume with points and assign points

within the wedge with the brightness temperature gradient, which looks like:

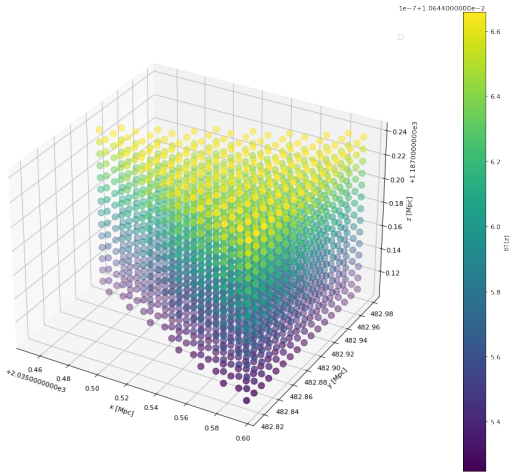

Figure 11: Points within wedge with an assigned brightness temperature gradient for a wake in comoving coordinates.

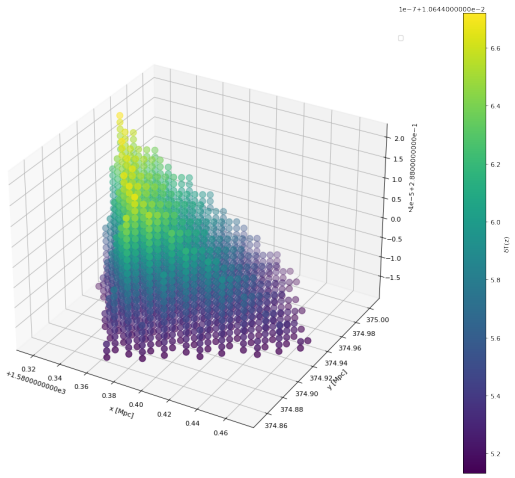

Figure 12: Points within wedge with an assigned brightness temperature gradient for a wake in comoving-redshift coordinates.

Now that we have our wake signal in comoving-redshift space, we can move onto including the noisy background onsent by cosmological ΛCDM perturbations and look at statistics to extract the signal.

6 Extracting the 21 cm signal from background maps

6.1 Match filtering maps

Before including a 3D noise map computed from early universe formation simulations, we first look at a 2D special cases or slices of the 3D case. Consider the following maps:

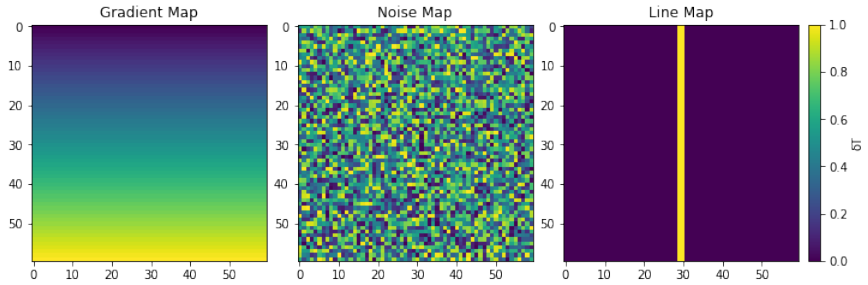

Figure 13: Brightness temperature maps slices along the vertical plane. The left map is the wake gradient map, the middle is a generic random noise map, and the right is an example of a map with a distinct line geometry.

We can go along each row and unfold the matrix containing the temperature values into a single array containing all the values. Moreover, we can also unfold vertically by going along the columns instead of the rows, which will be important in demonstrating the different look of the signal based on unfolding orientation. After unfolding the maps above we have something that looks like:

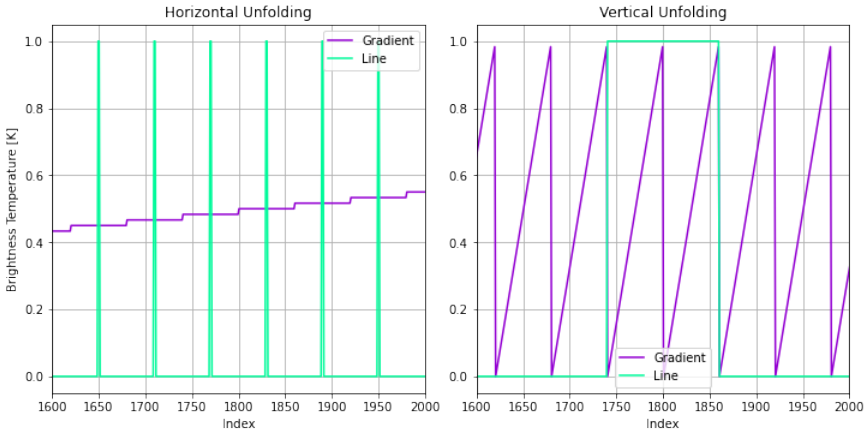

Figure 14: 2D temperature gradient and line maps unfolded horizontally (left) and vertically (right).

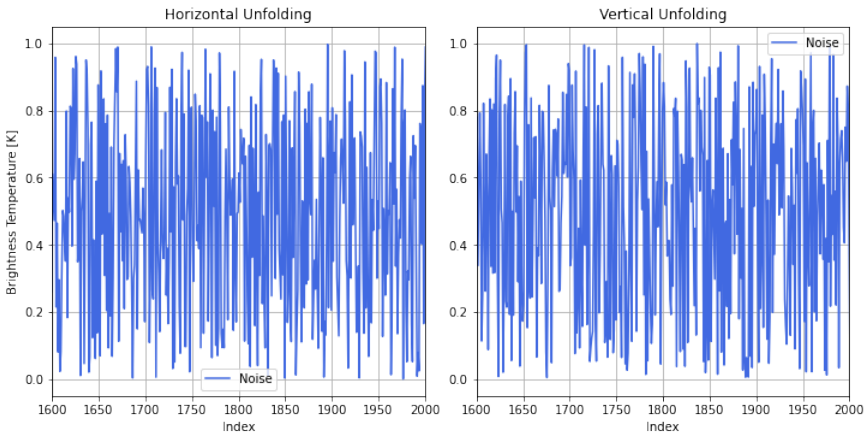

Figure 15: 2D temperature noise map unfolded horizontally (left) and vertically (right).

With this we can use our statistic for extracting the signal from the noise: match filtering. Since we unfolded we can use the 1D definition of match filtering given by [12]:

$$s(t) = \sum_{k=-n^2/2}^{n^2/2} h[t-k] \times d[k], \tag{22}$$

where h is the template or model array, in our case will be the wake gradient in a vacuum map, and d is the data which is being convolved with h. Here we see match filtering is simply a discrete convolution summing up the values at different index separations, which is a statistic that is particularly good at maximizing the signal to noise ratio. Using the definition above, we can compute the match filters for the different data samples in different unfolding orientations and result in:

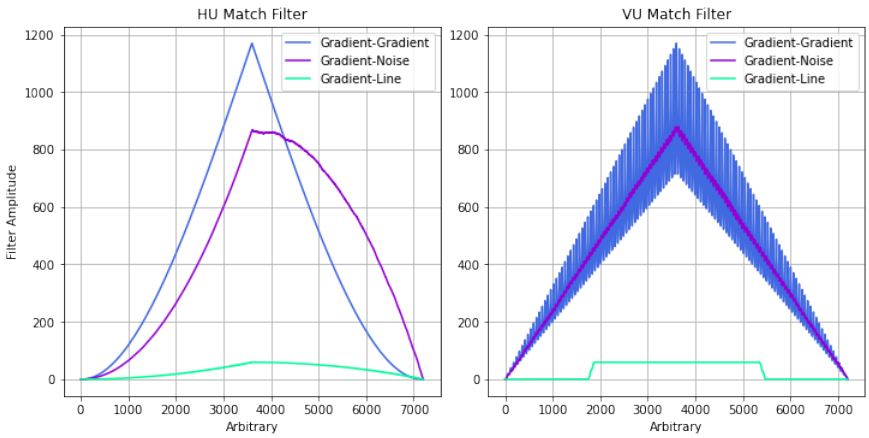

Figure 16: 1D match filtering for different data maps in various unfolding orientations. The left plot is for data that has been unfolded horizontally while the right plot is for vertical unfolding.

If we match filter the wake gradient with itself, meaning we would observe the wake in a vacuum, we are

left with the blue peaks as an ideal case. If we match filter the wake gradient with noise, we are left with the purple peaks that have a lower amplitude than the gradient filtered with itself. Thus, an observation of a wake in a background noise will have an amplitude that is bounded by the blue and purple curves. Moreover, we see the different unfolding orientations affect the filter amplitude, with the line signal being consistently suppressed.

We can alternatively compute match filtering for the 2D case without unfolding, which gives rise to the following plots:

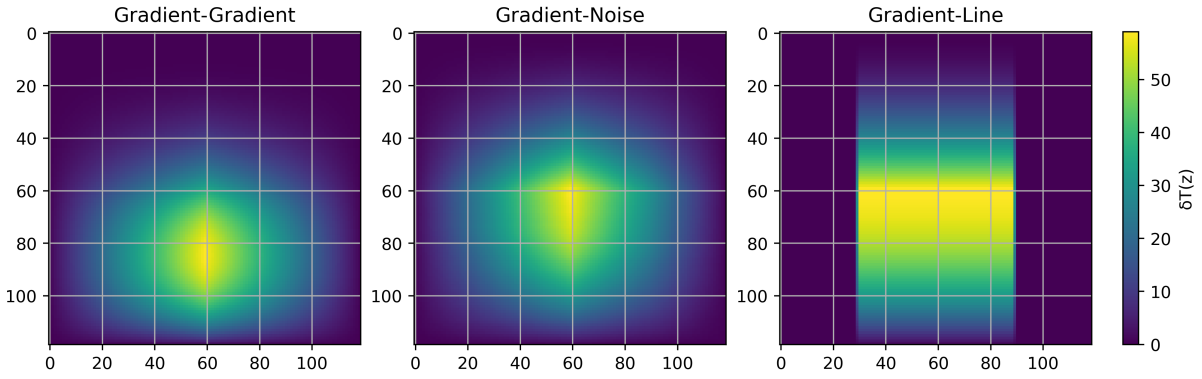

Figure 17: 2D match filtering for different data maps done using the scipy.signal.convolve2d function in Python.

As can be seen, the difference between the pure gradient filter with the gradient noise filter is more nuance than the 1D case. To elaborate the point further, we can unfold the 2D match filter in different orientations to compare the amplitudes, which results in:

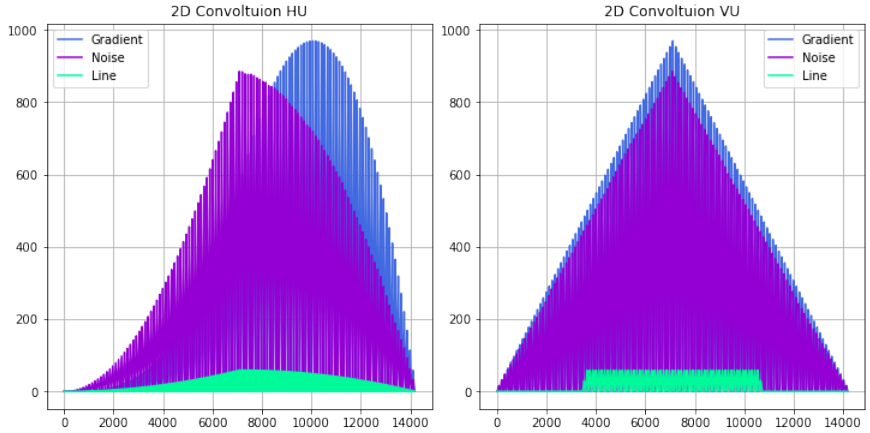

Figure 18: Unfolded 2D match filtering for different data maps. The left plot is for a match filter matrix that has been unfolded horizontally while the right plot is for vertical unfolding.

As can be seen above, the range of amplitude that a cosmological observation can be found is much tighter in the 2D case than the 1D case, thus we will proceed with 1D match filtering. Finally, we can use

this 1D match filtering method to compute the match filter between the string wake in physical-redshift space with the random noise map (normalized between 0 and 1), producing the following plot:

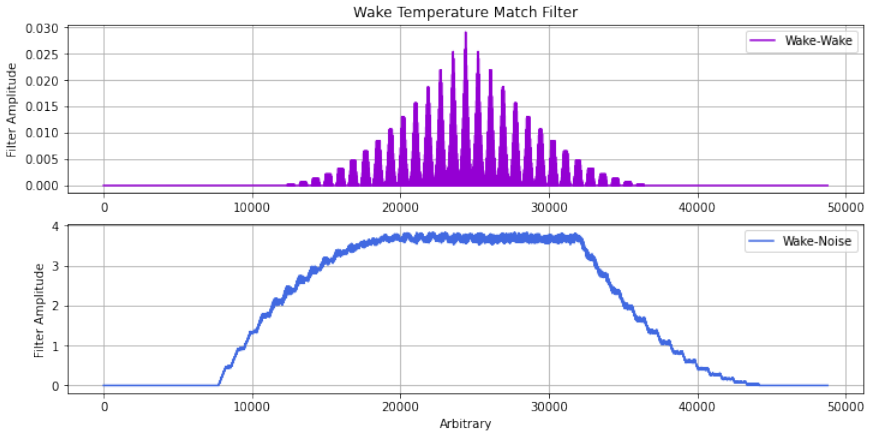

Figure 19: 1D match filtering of the 3D string wake and the noise map. In this case we use the full 3D wake temperature map from Fig. 12 and convolve is with the 3D analogue of the noise map in Fig. 13.

As can be seen above, there is a large difference is amplitude between the amplitudes of the match filter between a pure gradient filter, and a filter with a noise map. In the next section we plan on computing match filters along different lines of sight with a proper 3D ΛCDM noise map.

6.2 Match filtering along lines of sight

Now we consider superimposing the 3D wake signal map with the 3D ΛCDM noise map to perform more match filtering along different slices or lines of sight. First, we consider a ΛCDM noise map for a $200 \times 200 \times 200$ Mpc comoving box that is computed through 21cmFAST, a package used for computing cosmological simulations of physical fields in the early universe [14]. Furthermore, to match the size of our wedge map, we choose a $29 \times 29 \times 29$ Mpc section of the larger comoving box. Within this noise map, for each redshift we may slice along the xy-plane to consider different lines of sight, and perform statistics on each slice. For the sake of demonstration we consider the 9th, 10th, and 11th slice of the 29 Mpc slices. The slices for the 3D noise maps look like the following:

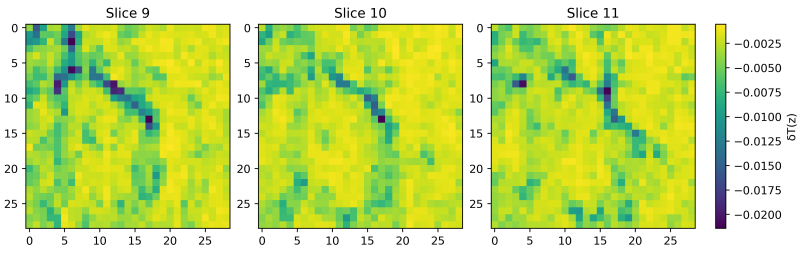

Figure 20: Line of sight slices of the ΛCDM cosmological perturbation map, with dimensions 29×29 Mpc.

Moreover, we can also pick the same index slices for our wake map, which looks like the following:

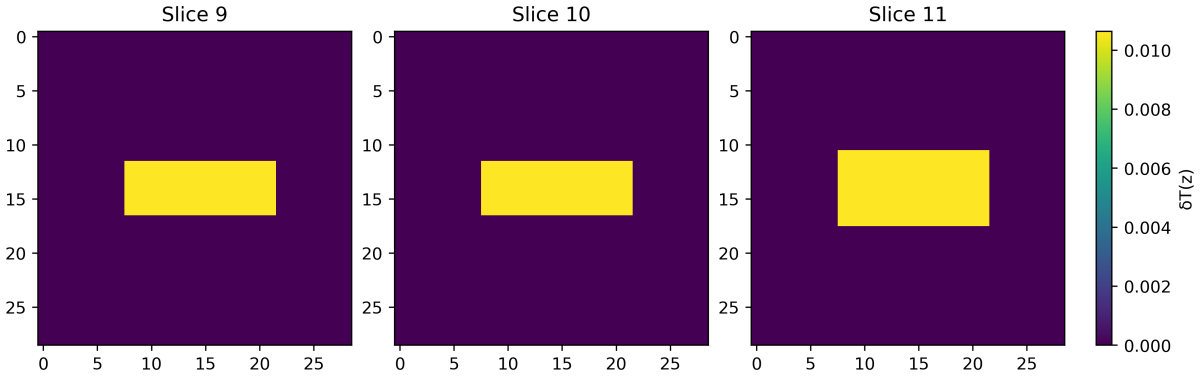

Figure 21: Line of sight slices of the string wake temperature map, with dimensions 29×29 Mpc. It is noted due to the small scale length, the temperature of the wake appears to be uniform in temperature but there is a small temperature gradient given by the brightness temperature. These will be our model parameters h which we convolve other maps with.

Finally, we can combine the maps to get the following set of combined plots:

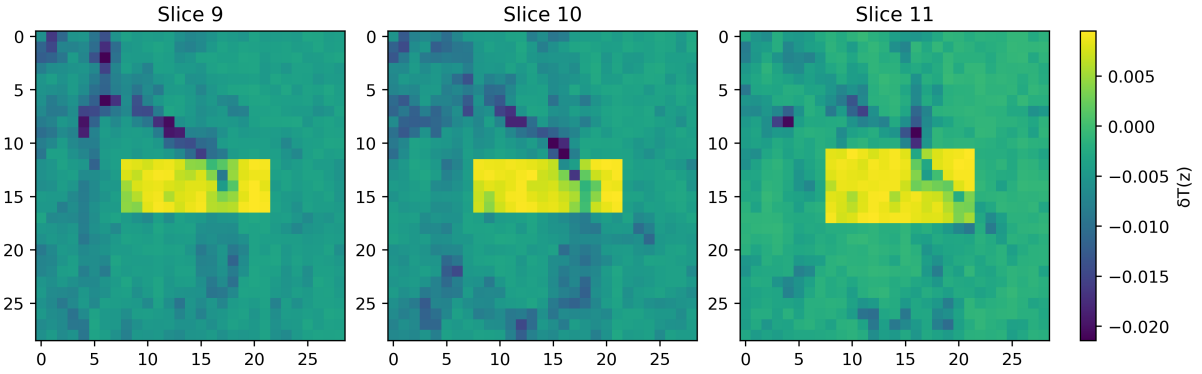

Figure 22: Line of sight slices of the combined string wake temperature and ΛCDM cosmological perturbation maps, with dimensions 29×29 Mpc.

From above, we can see at the string tension we are considering ($G\mu \sim 3 \times 10^{-7}$) that the string signal is visible by eye. The following statistics are thus useful when modulating the string tension, and the signal to noise ratio becomes suppressed. As before we perform match filtering convolutions to extract the signal from the combined maps. The following plots are the result of 2D convolutions between the different maps:

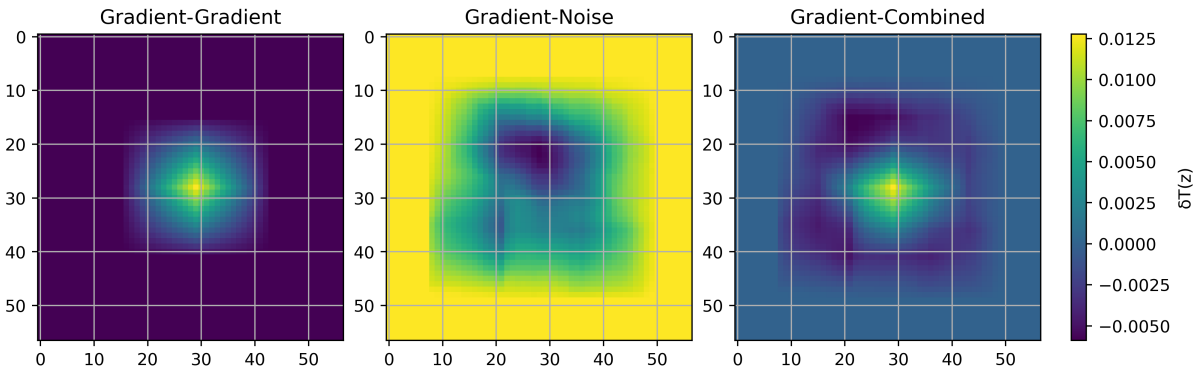

Figure 23: Result of 2D convolution of the different signal or noise maps with the string wake signal, done using the scipy.signal.convolve2d function in Python. The left most plot is the wake signal h convolved with itself, the middle plot is the wake signal convolved with the noise map, and the right most plot is the wake signal convolved with the combined wake-noise map.

As can be seen from above, the inclusion of the wake within the third combined map creates a peak within the 2D parameter space near the center where the wake is located. As done before, we can unfold these convolution maps into a 1D array and plot the temperatures, which look like the following:

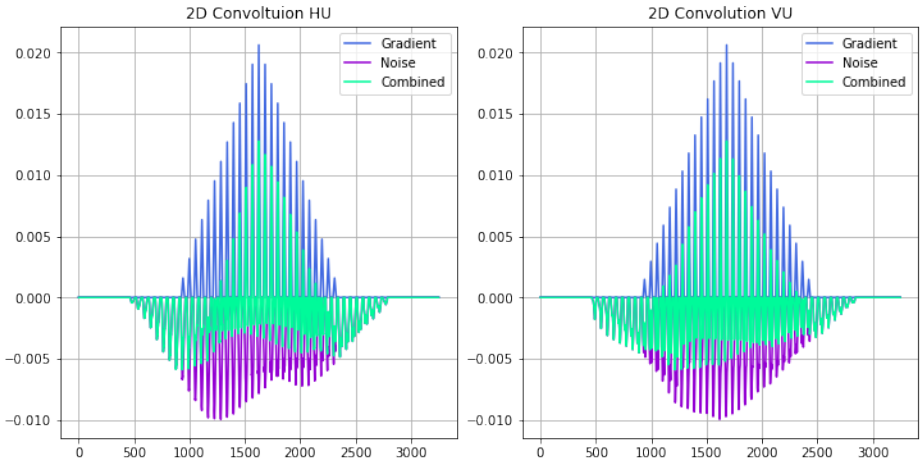

Figure 24: Result of 2D convolution of the different signal or noise maps with the string wake signal, unfolded in both horizontal (left) and vertical (right) orientations.

We see that the signal of a string wake in a vacuum is has the most prominent peak in blue, closely followed by the signal of a string wake in a noisy background in green. This means we expect the signal of a string wake in cosmological observations to be bounded by the blue and green curves. We can have a larger bound if we consider instead a 1D convolution of the maps. Consider unfolding the maps before convolution, which looks like the following:

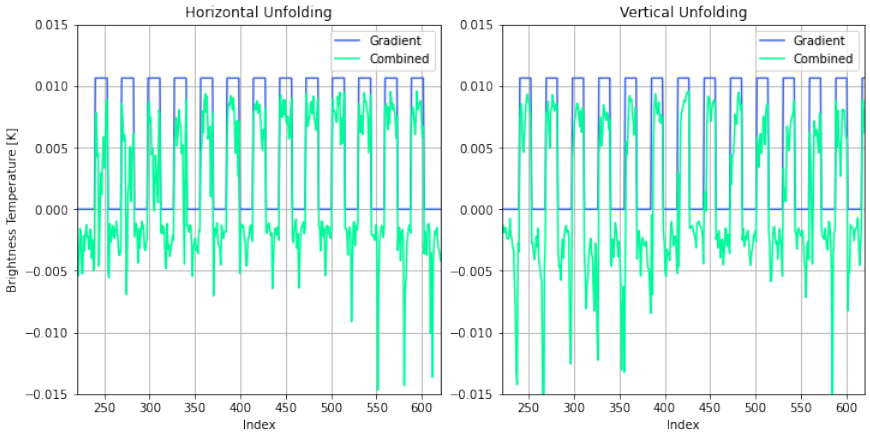

Figure 25: 2D temperature gradient and combined maps unfolded horizontally (left) and vertically (right).

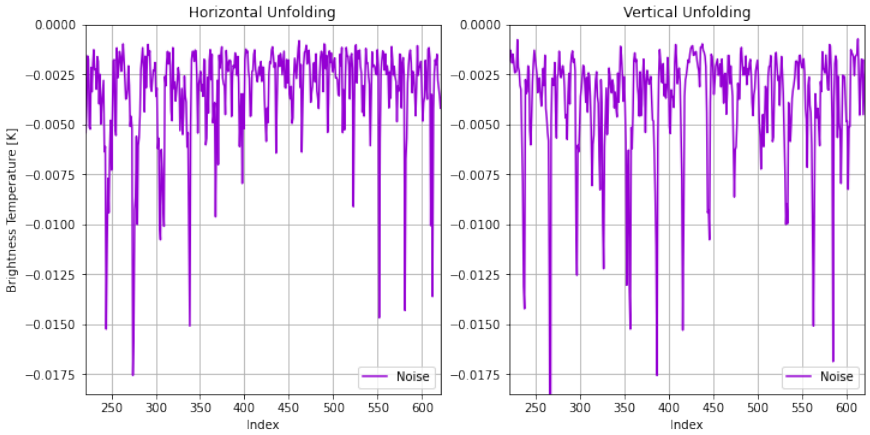

Figure 26: 2D temperature noise map unfolded horizontally (left) and vertically (right).

With the preceding unfolded maps, we can perform a 1D match filter to test the signal of the wake either in a vacuum or noisy background. The result of the 1D convolution is visualized in the following figure:

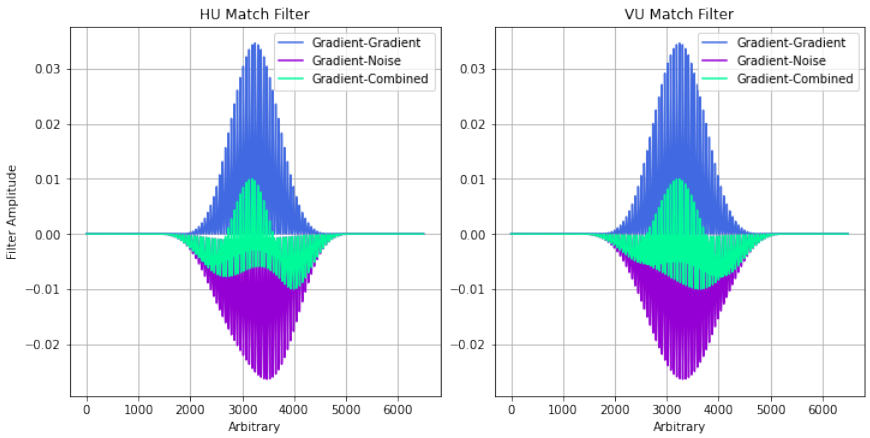

Figure 27: Result of 1D convolutions of the different signal or noise maps with the string wake signal, with the maps unfolded horizontally (left) and vertically (right) prior to the convolution.

As can be seen from above, the signal of the wake in a vacuum has a much higher amplitude compared to the noise as in the 1D case. This demonstrates a model in which we can employ statistics to able to extract the cosmic string wake signal from a noisy cosmological perturbation background map.

7 Caveats

It is worth mentioning some caveats of the analysis done above for those working on similar projects. First, the method in which points are detected within the wake is done using complex convex hulls. This algorithm becomes problematic when the blown up deficit angle is replaced by its actual value of $\alpha = 8\pi G\mu$ which is very small and thus the wake becomes a plane. The algorithm is based on connecting simplices along different vertices and does not work when the topology of the object is in 1D. Next, when converting from physical to comoving coordinates, one uses an inverse scaling factor of the form $a^{-1}(z) = (1-z)/z$, which can also be substituted for $a^{-1}(t_0) \sim 10^3$ for current observations. This scaling becomes an issue when wanting to scale physical axes to redshift axes using the numerical function from the astropy package, which doesn't converge for small ($\mathcal{O}(1)$) or large ($\mathcal{O}(1000)$) values of redshift. Thus, we are left with to work in a snapshot of physical coordinates to substitute for a continuous comoving coordinate system.

8 Conclusion

In this paper we developed a model and algorithm for extracting the signal of a U(1) topological defect (cosmic string wake) within a noisy cosmological perturbation background. We studied the mechanisms by which topological defects form within a non-Abelian quantum field theory and how homotopy groups are used to classify the stability of the defect. We then focused our attention to cosmic strings and looked at the construction of their wake in physical-redshift space. Furthermore, we demonstrated how to construct the temperature gradient and noise maps in comoving-redshift space. Finally, we looked at statistics for

extracting the cosmic string signal from a noisy background using match filtering, a convolutional statistic which maximizes the signal to noise ratio. It is found in the regime $G\mu \sim 3^{-7}$ that a 1D match filter after unfolding the temperature matrix into an array shows a clear indication for what a string signal observation looks like. We also demonstrate the domain in which the string signal is bounded by. We also mention some caveats of the analysis, including the limitation of numerical scaling convergence, and the thin geometry of the wake.

References

[1] N. D. Mermin. The topological theory of defects in ordered media. *Reviews of Modern Physics*, 51(3):591–648, July 1979.

[2] Michael Edward Peskin and Daniel V. Schroeder. *An introduction to quantum field theory*. Addison-Wesley Pub. Co, Reading, Mass, 1995.

[3] John C. Baez and Javier P. Muniain. *Gauge fields, knots and gravity*. World scientific, 1994.

[4] Robert H. Brandenberger. Topological Defects and Structure Formation. *International Journal of Modern Physics A*, 09(13):2117–2189, May 1994. arXiv:astro-ph/9310041.

[5] Ronald Brown, Philip J. Higgins, and Rafael Sivera. *Nonabelian algebraic topology: filtered spaces, crossed complexes, cubical homotopy groupoids*. Number 15 in EMS tracts in mathematics. European Mathematical Society, Zürich, 2011. OCLC: ocn724312753.

[6] Allen Hatcher. *Algebraic topology*. Cambridge University Press, 2019.

[7] T. W. B. Kibble. Classification of Topological Defects and Their Relevance to Cosmology and Elsewhere. In Yuriy M. Bunkov and Henri Godfrin, editors, *Topological Defects and the Non-Equilibrium Dynamics of Symmetry Breaking Phase Transitions*, pages 7–31. Springer Netherlands, Dordrecht, 2000.

[8] Robert H. Brandenberger. Searching for Cosmic Strings in New Observational Windows. *Nuclear Physics B - Proceedings Supplements*, 246-247:45–57, January 2014. arXiv:1301.2856 [astro-ph, physics:gr-qc, physics:hep-ph, physics:hep-th].

[9] T. W. B. Kibble. Symmetry breaking and defects, November 2002. Number: arXiv:cond-mat/0211110 arXiv:cond-mat/0211110.

[10] P. H. Frampton. Consequences of vacuum instability in quantum field theory. *Physical Review D*, 15(10):2922–2928, May 1977.

[11] Alexander Vilenkin. Gravitational field of vacuum domain walls and strings. *Phys. Rev. D*, 23:852–857, Feb 1981.

[12] Matteo Blamart, Hannah Fronenberg, and Robert Brandenberger. Signal of Cosmic Strings in Cross-Correlation of 21-cm Redshift and CMB Polarization Maps, May 2022. Number: arXiv:2205.02725 arXiv:2205.02725 [astro-ph, physics:gr-qc, physics:hep-ph, physics:hep-th].

[13] David Maibach, Robert Brandenberger, Devin Crichton, and Alexandre Refregier. Extracting the Signal of Cosmic String Wakes from 21-cm Observations. *Physical Review D*, 104(12):123535, December 2021. arXiv:2107.07289 [astro-ph, physics:gr-qc, physics:hep-ph, physics:hep-th].

[14] 21cmfast. 21cmfast/21cmfast: Official repository for 21cmfast: A code for generating fast simulations of the cosmological 21cm signal.